Oil & Gas Science and Technology – Rev. IFP Energies nouvelles (2016) **71**, 49

DOI: 10.2516/ogst/2015035

Combustion, Performance and Emission Analysis of an Oxygen-Controlling Downsized SI Engine

J.X. Zhou[1], B. Moreau[2], C. Mounaïm-Rousselle[2] and F. Foucher[2]*

[1] College of Mechanical and Electrical Engineering, Wenzhou University, Wenzhou 325035 - PR China
[2] Université d'Orléans, laboratoire PRISME, 8 Rue Léonard de Vinci, 45072 Orléans - France
e-mail: zhoujxi@wzu.edu.cn - bruno.moreau@univ-orleans.fr - christine.rousselle@univ-orleans.fr - fabrice.foucher@univ-orleans.fr

* Corresponding author

Abstract *— In the present study, experiments were carried out in a single-cylinder downsized SI engine with different rates of oxygen (15% to 27% by volume in the total mixture of intake gases except fuel) and equivalence ratios (from 0.45 to 1). Therefore, the oxygen volume fraction is due to oxygen enrichment or nitrogen dilution. The study of the impact of controlling the oxygen concentration on the combustion characteristics and emissions was performed at 1 400 rpm, at several loads (Indicated Mean Effective Pressure (IMEP) from 400 to 1 000 kPa). For each operation point, the spark advance and the intake pressure were adjusted simultaneously in order to maintain the load and obtain a minimum value of the indicated Specific Fuel Consumption (SFC). The effect of the oxygen concentration on the engine combustion characteristics was simulated by using the commercial software AMESim, with the combustion model developed by* IFP Energies nouvelles*, and an adapted algorithm was used to avoid residual gas calibration. By implementing a correlation for the laminar burning velocity, the in-cylinder pressures were perfectly predicted with a maximum pressure relative error of less than 2% for almost all the operating points. The classification of engine combustion according to the Peters-Borghi diagram, gives a deeper insight into the interaction between turbulence and the flame front.*

Résumé — Combustion, performance et analyse des émissions d'un moteur essence suralimenté avec contrôle de l'oxygène admis — Dans cette étude, des expériences sur monocylindre essence suralimenté ont été réalisées avec comme variable le taux d'oxygène (15 % à 27 % en volume dans le mélange total de gaz d'admission à l'exception du carburant) admis et la richesse (0,45 à 1). La fraction volumique d'oxygène représente en fait soit un enrichissement en oxygène de l'admission moteur ou de l'azote de dilution. L'étude de l'impact du contrôle de la concentration d'oxygène sur les caractéristiques de combustion et les émissions a été effectuée à 1 400 tr/mn, pour plusieurs charges, de 400 à 1 000 kPa. Pour chaque point de fonctionnement, l'avance à l'allumage et la pression d'admission ont été ajustées simultanément afin d'obtenir la charge maximale et la valeur minimale de consommation spécifique indiquée de carburant. L'effet de la concentration en oxygène dans la combustion du moteur a été simulé à partir du logiciel AMESim, avec le modèle de combustion développé par l'*IFP Energies nouvelles*, et un algorithme adapté a été utilisé pour éviter l'étalonnage de gaz résiduels. À partir d'une corrélation pour la vitesse de combustion laminaire, les valeurs de pression cylindre ont été prédites avec une erreur relative inférieure à 2 %, pour tous les points de fonctionnement. Le classement de la combustion selon le diagramme de Peters-Borghi a permis d'avoir une idée plus précise de l'interaction entre la turbulence et le front de flamme dans ces conditions.

LIST OF SYMBOLS

CAD	Crank Angle Degree
CFD	Computational Fluid Dynamics
CFM	Coherent Flame Model
EGR	Exhaust Gas Recirculation
IMEP	Indicated Mean Effective Pressure
k	Turbulent kinetic energy
l_t	Integral length scale
m	Mass
P	Pressure
Q_{comb}	Heat release by combustion
r_{bg}	Mean radius of burnt gases
SFC	Specific Fuel Consumption
S_L^0	Laminar burning velocity
T	Temperature
UHC	Unburned HydroCarbon
u'	Instantaneous velocity fluctuation
V	Volume
V_{cyl}	Displacement volume of cylinder
W	Molar weight
Y	Mass fraction
ff	Flame front
pf	Post-flame
α	Correlation constant
β	Correlation constant
γ	Correlation constant
δ_l	Laminar flame thickness
ϕ	Equivalence ratio
ρ	Density
τ	Thermal expansion rate
σ_m	Mean flame surface
σ_t	Turbulent flame surface
χ	Volume fraction
υ	Stoichiometric coefficient
v_{O_2}	O_2 percentage in the air
Ξ	Flame front wrinkling factor

INTRODUCTION

The objective of this paper is to study the combustion of a downsized SI engine in the case of controlled oxygen concentration at the intake. On the one hand, oxygen-enriched combustion can improve engine power density with the same intake pressure level. Thus, oxygen-enriched combustion can be used either as a booster to increase engine output or as a combustion enhancer when the engine operates at low loads or in cold-start conditions. Several studies performed with oxygen enrichment in SI engines showed positive effects such as reduction of Unburned HydroCarbon (UHC) fuel and CO [1-4], optimization of the downsized operating mode due to the direct effect on the combustion process and overall engine thermodynamics [5], and a decrease in the combustion phase [6-8]. On the other hand, a low oxygen concentration in the air (or N_2 dilution) can be considered as an alternative to Exhaust Gas Recirculation (EGR), which has been widely investigated in recent years [9, 10].

The oxygen concentration in the air can be controlled by using elective permeation through a non-porous polymeric membrane. This kind of polymeric membrane is now extensively studied and was developed recently to solve a part of the CO_2 sequestration problem for fixed-site power generation, for example [6, 11, 12]. It would deplete or enrich oxygen in the intake air while being compact, lightweight, embeddable in the vehicle and inexpensive by overcoming the current problems of a loop EGR. Different from the current EGR dilution system, air is pre-selected to meet the N_2 dilution or O_2 enrichment level as desired for the oxygen controlled by the membrane. Then, the air is recomposed with oxygen enrichment or nitrogen dilution for engine applications [13].

The first purpose of this paper is to investigate experimentally the impact of controlling the oxygen concentration on engine performance and pollutant emissions, and to give a global overview of the optimized engine operating conditions with the lowest Specific Fuel Consumption (SFC) and exhaust gas emissions. In order to provide more details about the specificity of combustion processes with oxygen control, such as turbulent flame velocity evolution during the engine cycle or flame wrinkling, the AMESim commercial software with the combustion model developed by Richard *et al.* [14] was used. The AMESim software provides the following advantages: first, it enables the various physical domains involved in vehicle and engine system simulation to be addressed with a high level of detail [15]. Thanks to this advantage, an AMESim model can be set up with reference to the experimental configuration; for example, intake and exhaust pipes, engine valves, turbo-compressors, and so on. Secondly, the combustion model developed by Richard *et al.* [14] gives an accurate description of the physical processes. Although this combustion model is based on a weak assumption for the mean flame geometry, the combustion parameters (*i.e.* flame surface, turbulent intensity, laminar and turbulent burning velocities) provided by the model give a realistic physical meaning for the in-cylinder combustion process.

1 EXPERIMENTAL SETUP

1.1 Engine Characteristics

Experiments were carried out in a single-cylinder SI engine (*PSA* EP6) characterized by a four-valve pent-roof chamber

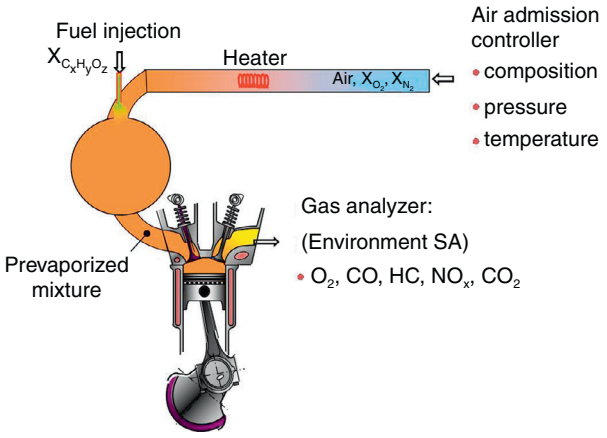

Figure 1

Scheme of air-fuel mixture system for the single-cylinder engine.

with a displacement volume (V_{cyl}) of 399.5 cm^3 and a compression ratio of 10.5. The bore, stroke and connecting rod lengths were 77 mm, 85.8 mm and 138.5 mm, respectively. The engine was driven by an electric motor at a fixed engine speed, and equipped with an optical encoder mounted on the main shaft, giving a 0.1 Crank Angle Degree (CAD) as resolution. A conventional spark plug with an electrode space of 1 mm was used. A timer card ensured synchronization of the various trigger signals and data acquisition systems. The engine sucks in the air through a thermal mass flowmeter and all other flows were evaluated from this reference flow. Oxygen, nitrogen and air flows were controlled by using thermal mass flow meters with an accuracy of ±0.7% for the instantaneous flow. Before the intake pipe, all the gases passed through a plenum volume, to avoid pressure oscillations inside the intake port. The isooctane quantity was regulated by using a 0-8 kg/h *Bronkhorst* Coriolis mass flow controller with a maximum combined standard uncertainty of ±1% for the minimum flow rate considered in the present work. To provide a premixed air-fuel mixture inside the intake pipe, the fuel was vaporized and mixed inside the intake pipe just after the plenum to obtain a homogeneous air-fuel mixture. The air-fuel mixture temperature was kept constant at 70°C by an electric heater. A scheme of the air-fuel injection system in the engine environment is presented in Figure 1.

Cylinder pressure was recorded with a water-cooled *AVL* quartz pressure transducer connected to a charge amplifier at 0.1 CAD resolutions. The linearity (<±0.6%) of the transducer was verified starting from a maximum pressure of 10 MPa (> maximum pressure in the engine). In this work, the absolute cylinder pressure was deduced by equalizing the in-cylinder pressure at 20 CAD after inlet valve opening timing to the intake mean absolute pressure. Thus, 100 consecutive cycles of cylinder pressure data were acquired by a PC equipped with a National Instruments acquisition board.

The exhaust emissions of gases (NO_x, HC, CH_4, CO, CO_2 and O_2) were measured by a classical emission analyzer (from *Environment S.A.*) with an accuracy <2% of the measured value and 1% of full scale.

1.2 Operating Conditions

Oxygen control was obtained by adding oxygen or nitrogen to ambient air. For simplification, we assume that the air consists of 21% O_2 and 79% N_2. To provide an O_2 percentage higher than 21%, O_2 was supplied by a compressed O_2 high-pressure tank. For an O_2 percentage less than 21%, N_2 was produced by an N_2 generator. Here, the percentage is defined as the volume fraction:

$$\chi_{O_2} = \frac{V_{O_2}}{V_{O_2} + V_{N_2}}.100\%$$

Thus, for $\chi_{O_2} > 21\%$, we have:

$$\chi_{O_2} = \frac{0.21V_{air} + V_{O_2}}{V_{air} + V_{O_2}}$$

with: $V_{air} + V_{O_2} = 1$.

For $\chi_{O_2} < 21\%$,

$$\chi_{O_2} = \frac{0.21V_{air}}{V_{air} + V_{N_2}}$$

with: $V_{air} + V_{N_2} = 1$.

The volume fraction of air, O_2 and N_2 can then be determined for a given O_2 percentage as shown in Table 1. The equivalence ratio φ was also predefined during experiments based on the quantity of oxygen and not on the quantity of air:

$$\phi = \frac{\text{stoichiometric } O_2/\text{fuel ratio}}{\text{actual } O_2/\text{fuel ratio}}$$

TABLE 1

Determination of the volume fraction of air, O_2 and N_2 for different cases

For $\chi_{O_2} > 21\%$	$V_{O_2} = \frac{\chi_{O_2} - 0.21}{0.79}$
	$V_{air} = \frac{1.21 - \chi_{O_2}}{0.79}$
For $\chi_{O_2} < 21\%$	$V_{N_2} = \frac{0.21 - \chi_{O_2}}{0.21}$
	$V_{air} = \frac{\chi_{O_2}}{0.21}$

TABLE 2
Correspondence between the O_2 rate and EGR percentage at the stoichiometric equivalence ratio

O_2 (%)	15	17	19	21	23	25	27
N_2-dilutio (%)	26.9	17.7	8.6	−0.3	−9.2	−17.9	−26.6

The global reaction of the isooctane/N_2/O_2 mixture can be defined as follows:

$$C_8H_{18} + \frac{12.5}{\phi}\left(O_2 + \frac{\chi_{N_2}}{\chi_{O_2}}N_2\right) \rightarrow \frac{8}{\phi}CO_2 + \frac{9}{\phi}H_2O + \frac{12.5}{\phi}\frac{\chi_{N_2}}{\chi_{O_2}}N_2 + M, \text{ for rich mixture}$$

$$\rightarrow 8CO_2 + 9H_2O + 12.5\frac{\chi_{N_2}}{\chi_{O_2}}N_2 + M, \text{ for lean mixture}$$

where M is the quantity of excess air or unburned fuel for lean or rich mixtures, respectively. Thus, for a given equivalence ratio ϕ, the fuel mass flow rate is directly linked to the O_2 mass flow rate.

In order to compare the O_2 rate with the EGR percentage for a fixed equivalence ratio, the equivalence between them was calculated by replacing the inert gases CO_2 and H_2O with N_2. For $O_2 < 20.9\%$, combustion takes place with N_2 dilution, and for $O_2 > 20.9\%$, with O_2 enrichment (or 'negative' dilution). An example of equivalence between the O_2 and N_2 dilution rates for a fixed equivalence ratio is presented in Table 2. Negative N_2 dilution corresponds to O_2 enrichment, which also means that the N_2 is 'removed' from the air. As many studies have been carried out with EGR, represented by N_2 dilution in this study, Table 2 facilitates comparison between our data and the data reported by other studies.

For the test, the IMEP was adjusted to keep a quasi-constant value, and the spark ignition was set at the optimum spark ignition timing, to allow lower SFC. The intake pressure was also adjusted during the operation, so that for a given equivalence ratio and O_2 percentage, the IMEP is adjusted by advancing the spark timing and intake pressure. The covariance value of the IMEP was used as a criterion in this study to determine the lean and N_2 dilution operating limits: a maximum of 5% was considered to be acceptable.

1.3 Studied Cases

The different operating points studied experimentally and numerically are presented in Figure 2a with various conditions of the IMEP and oxygen percentage for an air-fuel mixture at the stoichiometric equivalence ratio. In Figure 2b, for a fixed condition of 8 bar IMEP, the effect of different equivalence ratios was improved.

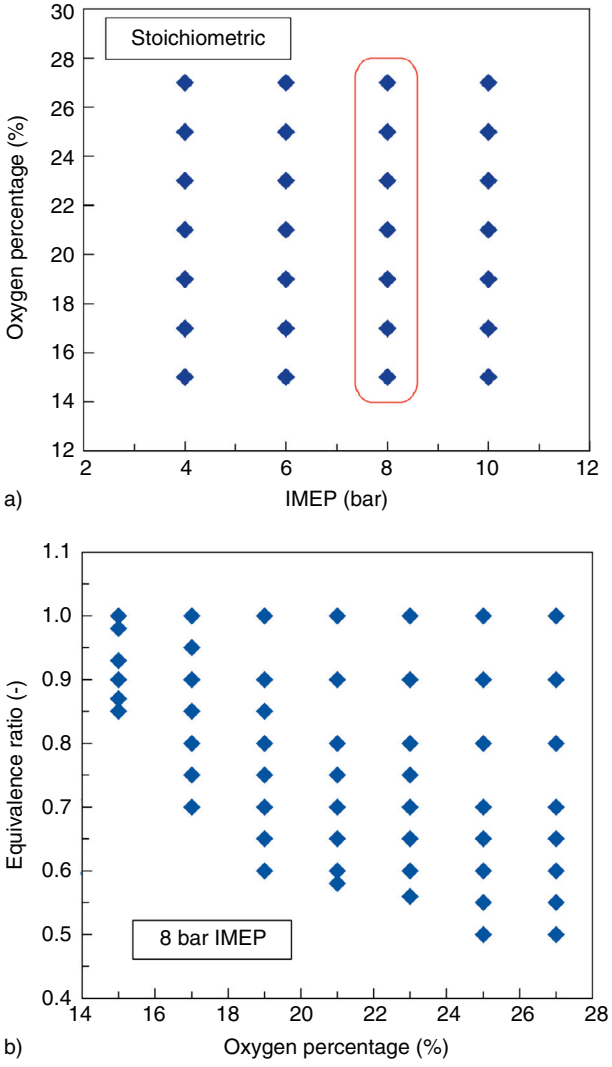

Figure 2
All different operating conditions were studied at fixed 1 400 rpm. a) In fixed stoichiometric conditions, b) in fixed 8 bar IMEP conditions.

2 DESCRIPTION OF THE MODEL

The combustion model used in this work is a physical 0D model, obtained by reduction of the 3D Coherent Flame Model (3D CFM) [14]. CFM formalism distinguishes two zones: fresh and burned gases, which are separated by a flame front propagating from the burned gases toward the fresh gas mixture. Chemical reactions of fuel oxidation

occur in the flame front, a very thin layer compared with all scales of the turbulent flow, and post-flame chemistry takes place in the burned gases. The main assumptions made to derive the 0D model are the following [14, 16]:

- in each zone, the mixture composition is assumed to be homogeneous and hence to have uniform properties;
- the pressure is uniform throughout the cylinder in both zones;
- the gaseous mixture consists of 15 species (Fuel, N_2, O_2, H_2, H_2O, CO, CO_2, NO, NO_2, HC, NH_3, soot, O, H and OH);
- the gases considered are ideal gases;
- the turbulent kinetic energy field is assumed to be uniform in the cylinder.

2.1 Heat Release Calculation

The enthalpy balance equations were described in detail in the previous study of Richard *et al.* [14]. The heat release by combustion is expressed as:

$$\frac{dQ_{comb}}{dt} = \sum_i h_{f_i} \left(\left.\frac{dm_i}{dt}\right|_{ff} + \left.\frac{dm_i}{dt}\right|_{pf} \right) \tag{1}$$

where h_{fi} is the formation enthalpy of species i, and $dm_i|_{ff}$ and $dm_i|_{pf}$ are the mass variations of this species, respectively, in the flame front (ff) and in the burned gases due to post-flame (pf) chemistry reactions. $dm_i|_{ff}$ can be expressed as a function of the fuel consumption rate:

$$\left.\frac{dm_i}{dt}\right|_{ff} = \upsilon_i \frac{W_i}{W_f} \left.\frac{dm_{fuel}}{dt}\right|_{ff} \tag{2}$$

where υ_i is the stoichiometric coefficient of gas i in the reaction of fuel oxidation through the flame, and W_i denotes the molar weight of this gas. The fuel consumption rate is then given by a flame propagation model described in the next paragraph. Finally, $dm_i|_{pf}$ is computed using a reduced chemistry approach [14] accounting for CO and NO formation in the burned gas zone.

2.2 Flame Propagation Model

The consumption rate of fuel throughout the flame front depends on the turbulent flame surface σ_t and the fresh gas properties according to:

$$\left.\frac{dm^{fg}_{fuel}}{dt}\right|_{ff} = -\rho_{fg} Y^{fg}_{fuel} S^0_L \sigma_t \tag{3}$$

where ρ_{fg} is the fresh gas density, $Y^{fg}_{fuel} = m^{fg}_{fuel}/m_{fg}$ is the fuel mass fraction in the fresh gases and S^0_L is the laminar burning velocity computed from a correlation, a function of the pressure and the fresh gas composition and temperature, described in the subsection below. The turbulent flame surface σ_t is written as the product of a mean surface σ_m and the flame front wrinkling factor, Ξ ($\sigma_t = \Xi\sigma_m$). The mean surface is computed by considering a spherical expansion of the flame from the spark plug to the cylinder walls in a realistic geometry. For this purpose, σ_m is *a priori* tabulated as a function of the burned gas volume and the piston position as described [14, 17]. The flame wrinkling factor evolution is described by a physical equation describing the progressive transition from the laminar kernel to the fully turbulent flame. This equation was obtained by reduction of the 3D equation for the flame surface density [18, 19] and includes the unsteady effect of the turbulent flow on the flame stretch through the efficiency function Γ proposed in [20]:

$$\frac{1}{\Xi}\frac{d\Xi}{dt} = \Gamma\left(u'/S^0_L,\, l_t/\delta_l\right)\frac{u'}{l_t}\left(\frac{\Xi_{equ} - \Xi}{\Xi_{equ} - 1}\right) - \frac{2}{r_{bg}}(1+\tau)(\Xi - 1)S^0_L \tag{4}$$

u' is the instantaneous velocity fluctuation, l_t is the integral length scale, δ_l is the laminar flame thickness estimated using Blint's correlation [21], $\tau = \rho_{fg}/\rho_{bg}$ is the thermal expansion rate, $r_{bg} = (3V_{bg}/4\pi)^{1/3}$ is the current mean radius of burnt gases and Ξ_{equ} corresponds to the Ξ value when an equilibrium is reached between turbulence and flame wrinkling Ξ [18]. The main unknowns of the problem finally correspond to the turbulent flow field properties u' and l_t.

2.3 Turbulence Model

The integral length scale is assumed to be close to the piston-cylinder head distance D, as proposed by many authors [17, 22], while $u' = \sqrt{2/3k}$ is obtained from a classical two- equation model describing the evolution of the mean and turbulent kinetic energy (resp. K and k) [14]. This model accounts for energy transfer from the mean flow into turbulence during the compression stroke and for dissipation of k on the Kolmogorov scale. Such a 0D model cannot be entirely predictive as the complex flow field evolution highly depends on the engine geometry and cannot directly be resolved as in 3D CFD calculations. Classically, the parameters of the turbulence model such as the integral length scale and the tumble number are then usually adjusted.

2.4 Adaptation of the AMESim Model for the Case of an 'Oxygen-Controlled Engine'

Figure 3 presents the sketch of the AMESim model. On the left is the intake part, in the middle the main engine block,

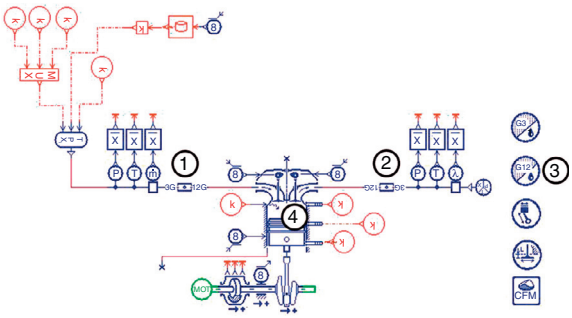

Figure 3

Scheme of AMESim modeling for an oxygen ratio-controlled engine.

containing the model of the intake and exhaust valves, the model of the 12 gases, the engine model, and on the right the exhaust part.

In this AMESim model, four parts of the subroutine (marked as ① to ④) were modified to adapt the oxygen control calculation using an advanced AMESim tool, called 'AMESet':

- ① and ② are pipe models which transform the mixture of 3 gases (air, fuel and burned gases) into 12 species (fuel, N_2, O_2, H_2, H_2O, CO, CO_2, NO, NO_2, HC, NH_3 and soot) when gases pass though the intake or exhaust pipes to the engine block. Inversely, from the engine block to the intake or exhaust side, 12 gases are transformed into 3 gases. In the pipe model, an integer parameter for the O_2 mole percentage was defined; thus, by changing this parameter to above or less than 21%, the air can be considered as oxygen-enriched or nitrogen-diluted, respectively;
- ③ is the model of the 12 gas engine fluid data, where instead of a stoichiometric air-fuel ratio, a stoichiometric oxygen-fuel ratio is calculated to determine the equivalence ratio based on oxygen, as defined in the previous section;
- ④ the engine combustion model, was changed by using the integer parameter for the O_2 mole percentage to control the oxygen percentage in the air and as a variable for laminar burning velocity correlation and auto-ignition delay time correlation.

2.5 Laminar Burning Velocity Correlation

The laminar burning velocity for different quantities of O_2 was experimentally investigated in previous studies [23, 24]. In order to take into account the effect of oxygen control on the engine combustion simulation, a correlation based on an experimental estimation [24] was implemented in the AMESim model:

$$S_L^0 = S_{Lref}^0 \left(\frac{T_i}{T_{ref}}\right)^{\alpha_s} \left(\frac{P_i}{P_{ref}}\right)^{\beta_s}$$

In the above relationship, S_{Lref}^0 is a function of the equivalence ratio:

$$S_{Lref}^0 = A + B(\phi - \phi_m) + C(\phi - \phi_m)^2 + D(\phi - \phi_m)^3 + E(\phi - \phi_m)^4$$

and,

$$\alpha_s = \alpha_1 + \alpha_2(\phi - \phi_m)$$

$$\beta_s = \beta_1 + \beta_2(\phi - \phi_m)$$

T_{ref} and P_{ref} are the reference temperature and pressure, respectively and S_{Lref}^0 the laminar burning velocity of these conditions. In this correlation, pressure, temperature and laminar burning velocity are respectively expressed in bar, K and cm/s.

In the study of Galmiche *et al.* [24], an empirical term was added to take into account both the effect of N_2 dilution and O_2 enrichment:

$$S_L^0(v_{O_2}) = S_L^0(v_{O_2 ref}) \left(\frac{v_{O_2}}{v_{O_2 ref}}\right)^{\gamma}$$

where $\gamma = \gamma_1 + \gamma_2(\phi - \phi_m)$, with two constant values of γ_1 and γ_2. v_{O_2} is the percentage in the air defined by:

- in the case of N_2 dilution:

$$v_{O_2} = \frac{n_{O_2(synthetic\ air)}}{n_{O_2(synthetic\ air)} + n_{N_2(synthetic\ air)} + n_{N_2(diluent)}}.100$$

- in the case of O_2 enrichment:

$$v_{O_2} = \frac{n_{O_2(synthetic\ air)} + n_{O_2(enrichment)}}{n_{O_2(synthetic\ air)} + n_{N_2(synthetic\ air)}}.100$$

$v_{O_2 ref}$ is the reference percentage of O_2 in the air, *i.e.* the percentage of O_2 in the synthetic air.

The parameters used in the correlation are listed in Table 3.

In order to apply this correlation to the engine combustion calculation, the effect of residual gas can be defined by:

$$S_L^0(v_{O_2}) \text{ with residual gas} = S_L^0(v_{O_2})(1 - 2.1\chi_{residual})$$

where $\chi_{residual}$ is the residual gas proportion inside the cylinder.

TABLE 3
Correlation parameters used to estimate laminar burning velocity

Parameter	Optimized value
A	56.21
B	−14.44
C	−214.08
D	43.47
E	267.17
α_1	1.88
α_2	−0.19
β_1	−0.24
β_2	0.27
γ_1	2.67
γ_2	0.17
ϕ_m	1.07

2.6 Calibration Process

The calibrations were accomplished by coupling AMESim with a Matlab program, to input experimental results in the requisite format.

Figure 4 illustrates the simulation process for all the engine operating points. First, experimental data (such as intake pressure, intake temperature, exhaust pressure, exhaust gas temperature, equivalence ratio, advanced ignition crank angle and in-cylinder pressure) are read by a Matlab program. In this program, Matlab-AMESim coupling was used to optimize the in-cylinder data.

The second part of this algorithm focuses on two-zone AMESim model simulation with oxygen control. In this part, the AMESim development tool, AMESet, was applied to induce laminar burning velocity as a sub-routine inside the main combustion model. In addition, the main two-zone combustion model was modified to adapt it to the oxygen control.

Multi-cycle simulations were performed with the initial 'guess value' of the integral scale and tumble value, and then the simulation results of in-cylinder pressure of the last simulation cycle were compared with the experimental data for a range of crank angles from 250 to 450 CAD. The discrepancy between the two values can be calculated by:

$$\text{error} = \sum_{i=250^\circ\text{CA}}^{450^\circ\text{CA}} \left(P_{cyl}(\text{simu}) - P_{cyl}(\text{expe})\right)^2 + \alpha * \left(P_{max}(\text{simu}) - P_{max}(\text{expe})\right)^2$$

The second term of the above expression gives a more precise P_{max} calibration with regard to the importance of P_{max} for heat release and exhaust gas emission. The parameter α gives a flexible value for considering the greater or lesser effect of P_{max}. Once the error between simulation and experimental in-cylinder pressure data is minimized, the value of l_t and N_{tumble} can be obtained by loop calculation. Finally, the above l_t and N_{tumble} maps were used to analyze the simulation results.

The present algorithm differs from the calibration process methodology employed by Richard *et al.* [14] using 'IFP-Optilab'. In the present study, the initial conditions that

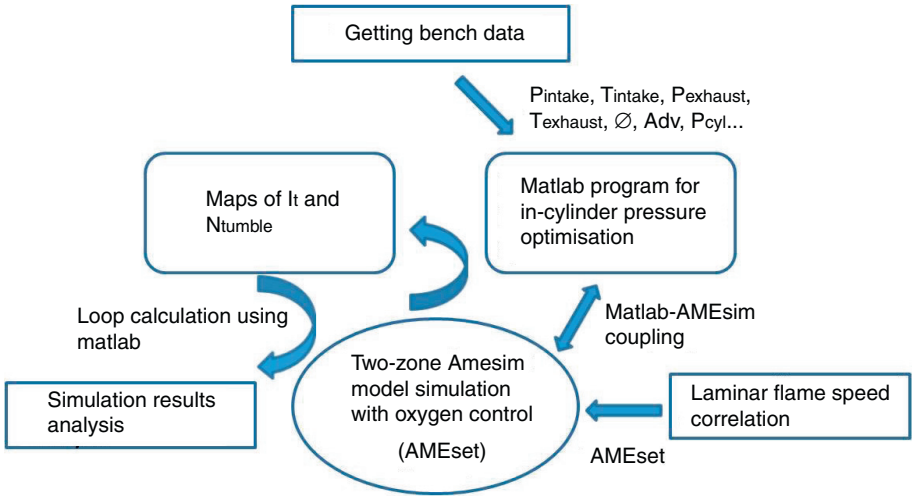

Figure 4
Global scheme of different simulation and model coupling and looping.

concern the mass fraction of air and of isooctane fuel, intake pressure and temperature are taken directly from experimental data. Residual burned gases, which have a significant impact on the combustion process (heat release, knock, pollutants, etc.), were estimated by a multi-cycle simulation with five real engine cycles. Only the results of the last cycle were used to calculate the error between in-cylinder simulation and experimental data and to analyze the results.

3 RESULTS AND DISCUSSION

3.1 Experimental Results

3.1.1 Fuel Consumption

The evolution of indicated SFC *versus* the equivalence ratio is presented in Figure 5 for different IMEP (400 kPa, 600 kPa, 800 kPa and 1 000 kPa). In these figures (Fig. 5a-d), the O_2 percentage in the air varies from 15 to 27%. For each O_2 percentage, the equivalence ratio is decreased to reach the lean operating limits. With the decrease in the equivalence ratio, SFC was decreased for a fixed O_2 percentage, although an SFC increase is usually observed at the operating limits.

For IMEP 400 kPa and 600 kPa (Fig. 5a, b), by increasing the O_2 percentage in the air and decreasing the equivalence ratios, a lower SFC can be obtained. Compared with the conventional operating point (with 21% O_2, and a stoichiometric case), SFC can be reduced by 15%. The lowest SFC is found at an O_2 percentage of around 25% to 27% with an equivalence ratio of 0.5 to 0.55, which means that oxygen-enriched combustion with a low equivalence ratio can be a potential method for improving fuel efficiency.

For IMEP 800 kPa (Fig. 5c), and an O_2 percentage from 15% to 19%, a lower SFC can be obtained by increasing the O_2 percentage while reducing the equivalence ratio, which is similar to the cases of IMEP 400 kPa and 600 kPa. However, for an O_2 percentage from 21% to 27%, this tendency is reversed. The lowest SFC for IMEP 800 kPa is found at 19% O_2 with an equivalence ratio of 0.7.

For IMEP 1 000 kPa (Fig. 5d), the lowest SFC is obtained at 15% O_2 with an equivalence ratio of 0.9. In this case, the dilution of N_2 will be a better way than oxygen enrichment to limit fuel consumption. Compared with the regular operating point (with 21% O_2, and a stoichiometric equivalence ratio), N_2 dilution has the potential to achieve about 10% fuel economy.

It can therefore be concluded that for low IMEP (400 kPa, 600 kPa), oxygen enrichment is a potential way to improve fuel efficiency, whereas for high IMEP (800 kPa, 1 000 kPa), N_2 dilution should be used to have a better fuel economy.

3.1.2 HC Emissions

Figure 6 represents the evolution of indicated specific HC emissions *versus* the equivalence ratio for two different IMEP (400 kPa, 1 000 kPa). The effect of oxygen enrichment on HC emissions is obvious. For each fixed equivalence ratio, the HC emission decreases with the increase in the O_2 percentage and the lowest values are always found at 27% O_2. Oxygen enrichment can decrease the quenching distance of the mixture. In the study by Friedman and Johnston [25], the quenching distance was found to be a decreasing function of the flame temperature, and it is well known that the flame temperature increases in the case of oxygen enrichment [23]. Mazas *et al.* [26] also showed that quenching effects at the flame front are reduced due to the increase in the flame temperature when the oxygen-enrichment ratio is increased. Thus, oxygen enrichment allows the flame to propagate much closer to the cylinder walls than the N_2 dilution mixture.

The specific HC emission increases when the equivalence ratio varies from 0.9 to 1; however, the HC emission decreases from the lean limits to an equivalence ratio of 0.9. The lowest value can be found around an equivalence ratio of 0.9.

3.1.3 NO_x Emissions

The evolution of NO_x emissions *versus* the equivalence ratio is presented in Figure 7. Contrary to HC emissions, at a fixed equivalence ratio value, NO_x emissions increase when the oxygen percentage is increased, with the exception of a few points which may be due to measurement error. As the formation of NO_x depends mainly on the burned gas temperature, due to the thermal formation process, the higher the burned gas temperature, the higher the rate of NO_x formation. Thus, the higher emission of NO_x for oxygen enrichment can be explained by the high temperature of the burned gases. The stoichiometric engine operating conditions show a slight decrease in NO_x emissions for the highest O_2 volume fraction, contrary to the literature. This is probably due to different reasons: as the later spark timing changes the thermodynamic conditions, it may have a significant effect on NO_x, especially at 10 bar IMEP, for 27% O_2, where the spark timing is retarded to prevent the knock. Moreover, although the O_2 enrichment produces a higher burned gas temperature and then causes higher NO_x emission, a lower concentration of N_2 is not conducive to NO_x formation. In the case of a highly lean mixture, the leaner the mixture is, the less NO_x emission it gets, even though the SFC is greatly increased (the lean limit points in Fig. 5). In the case of a lean mixture, the leaner the mixture is, the less NO_x emission it gets; the interval of the operation points for the equivalence ratio is normally set to 0.05, which may be too high, and induces the fluctuation of NO_x emissions. As shown in the

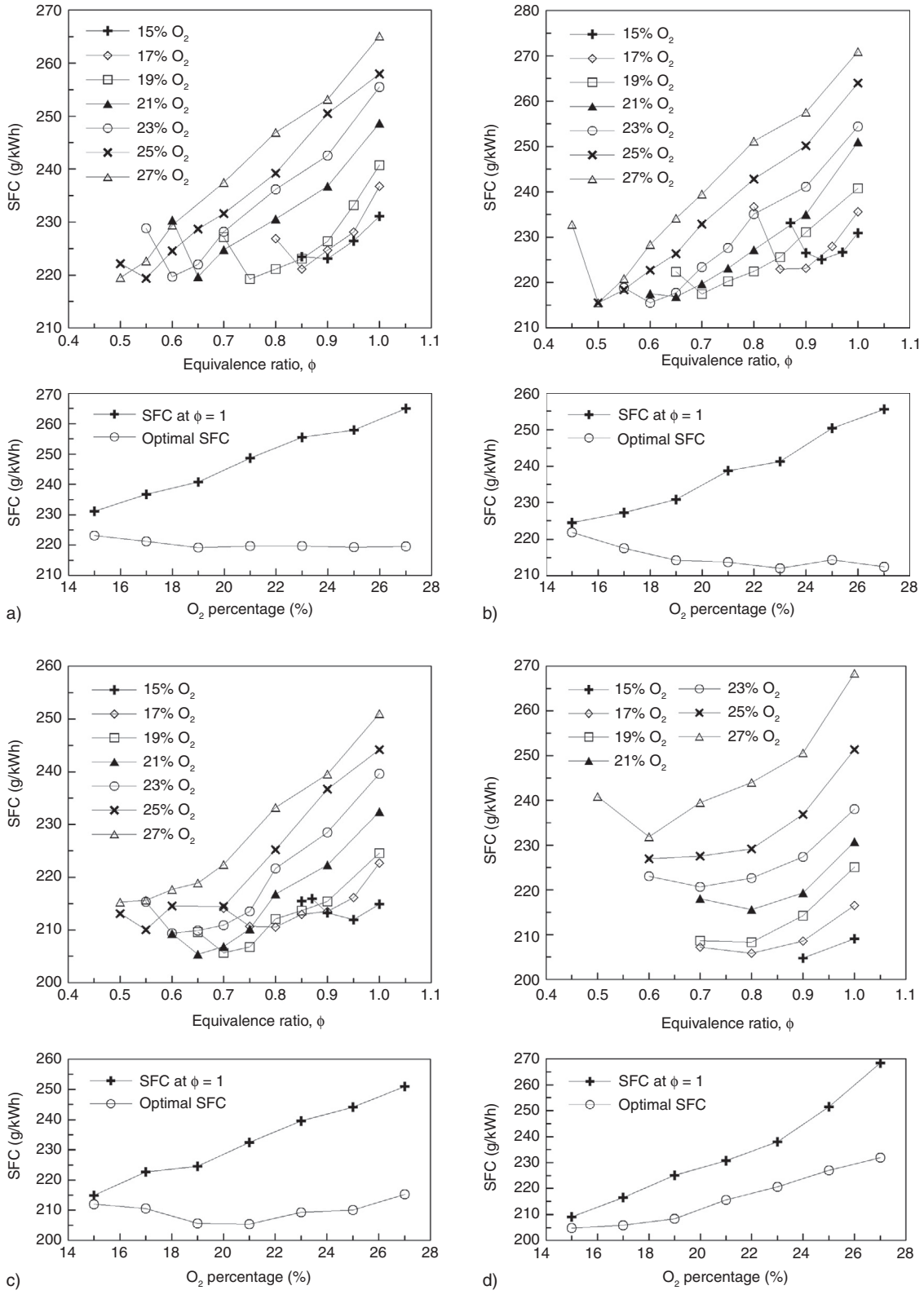

Figure 5

Evolution of indicated SFC *versus* the equivalence ratio for different IMEP; a) 400 kPa, b) 600 kPa, c) 800 kPa, d) 1 000 kPa.

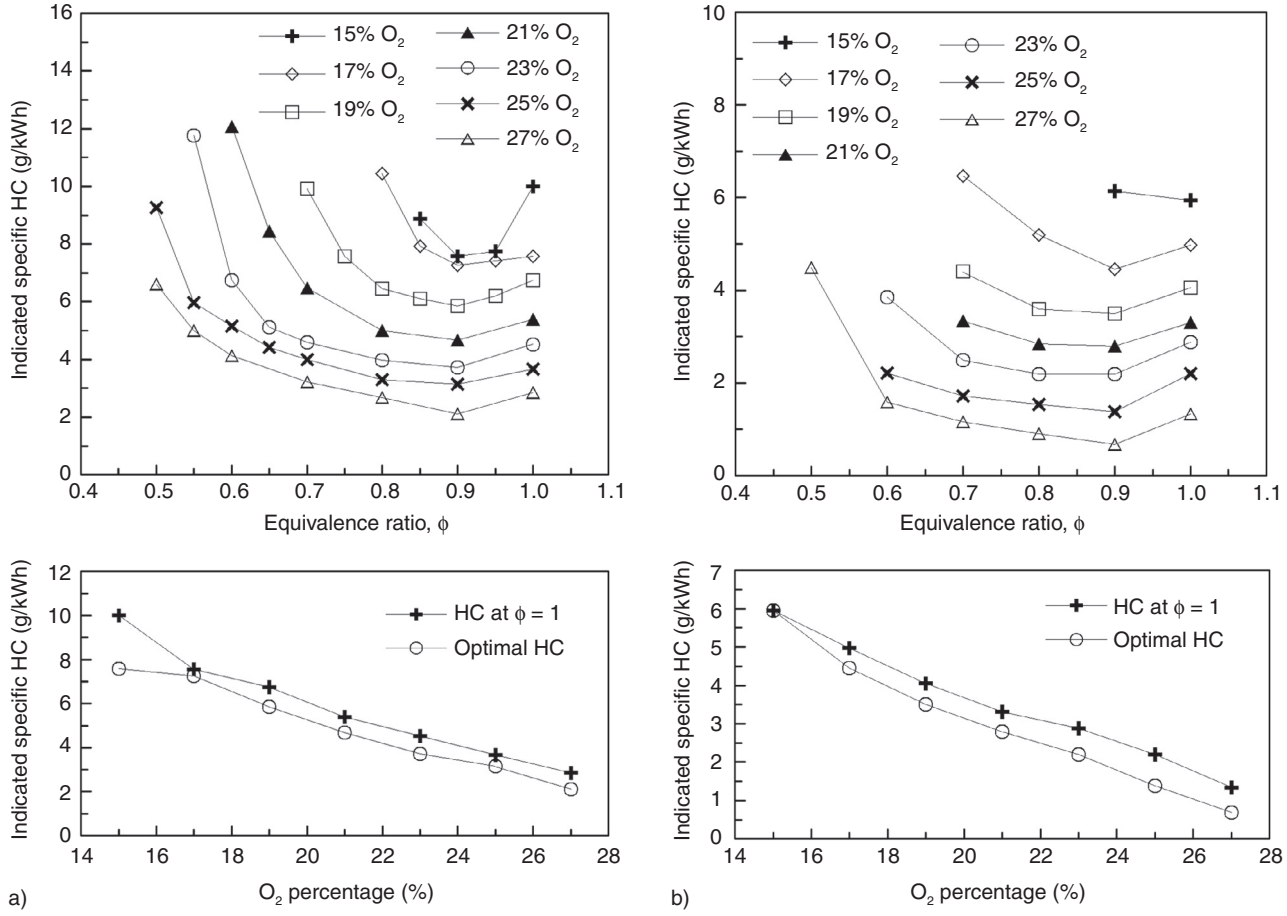

Figure 6

Evolution of indicated specific HC emissions *versus* the equivalence ratio for different IMEP; a) 400 kPa, b) 1 000 kPa.

lower part of Figure 7a, the filled circles represent the NO_x with high SFC (the lean limit points in Fig. 5a). The closer the lean limit is touched, the lower the NO_x emission.

3.1.4 CO Emissions

Figure 8 represents the evolution of indicated specific CO emissions *versus* the equivalence ratio for different IMEP (400 kPa, 1 000 kPa). CO emissions are mainly affected by the equivalence ratio ϕ; especially for ϕ near unit value, they decrease in lean conditions due to the increase in the O_2 concentration, which helps the oxidation of CO into CO_2. Compared with the equivalence ratio, the O_2 percentage in the air does not present a clear tendency. In Figure 8a, the local slope of the equivalence ratio between 0.95 and 1 for 17% O_2 can reach 240 (the closer it is to the unit ϕ value, the greater it is), which means that with one percent variation in the equivalence ratio, the CO emission will have more than 2.4 g/kWh discrepancy. Conversely, the biggest variation from 15% to 27% O_2 is about 7 g/kWh. Thus, to ensure precise CO measurement, the equivalence ratio should be controlled and the precision of the mass flow meters of fuel and gases should be checked.

3.2 ENGINE MODEL RESULTS

3.2.1 Engine in-Cylinder Pressure

Experimental and simulated in-cylinder pressure curves for different engine loads at 1 400 rpm are presented in Figure 9. The in-cylinder pressure evolution is plotted for different cases of the oxygen percentage at a stoichiometric equivalence ratio, 15% O_2, 21% O_2 and 27% O_2, respectively. The discrepancies can be found in Figure 9a, especially for

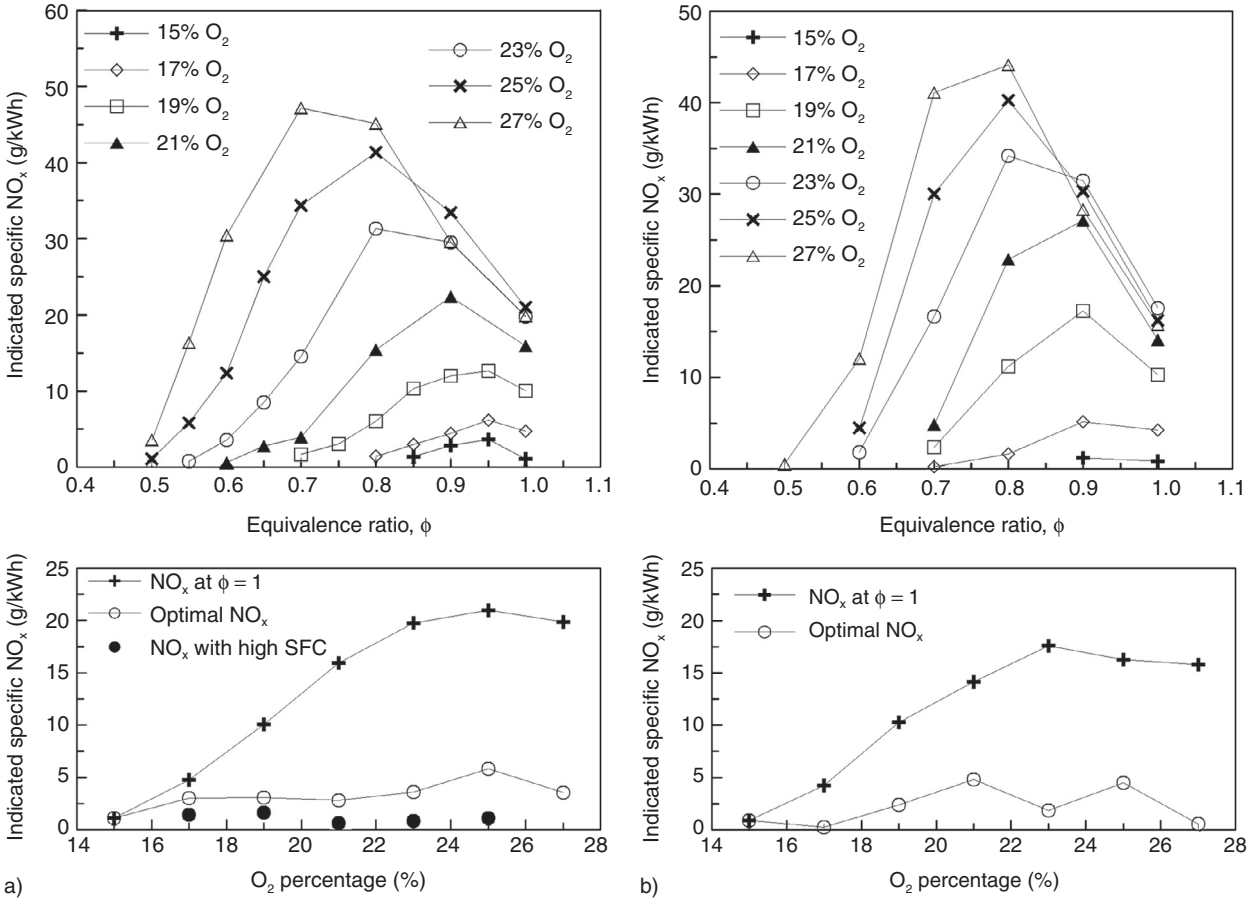

Figure 7

Evolution of indicated specific NO_x emissions *versus* the equivalence ratio with different IMEP; a) 400 kPa, b) 1 000 kPa.

the cases of IMEP 8 and 10 bar, which may be due to the assumption of spherical flame propagation inside the combustion volume. For a high nitrogen dilution mixture, the flame evolution in the cylinder becomes irregular, as previously observed by Mounaïm-Rousselle *et al.* [9]. However, good calibration results can be found in Figure 9b, c for 21% and 27% of O_2, respectively. The simulated results show good agreement with our experimental data, which indicates that the evolution of the burning velocity and therefore the heat release rate is well described for all cases [16].

In Figure 10, the IMEP absolute error and maximum pressure relative error *versus* the O_2 percentage for different cases of IMEP are presented. For all cases, IMEP relative errors do not exceed 3.5% and maximum pressure relative errors are less than 2%. The largest values of these errors are found at 15% O_2 and the smallest at an O_2 percentage above 21%. The maximum pressure relative error roughly decreases with increasing O_2 percentage.

In Figure 11, the integral length and the tumble number *versus* the O_2 percentage are presented for IMEP from 400 to 1 000 kPa. As these two parameters are used to adjust the simulation, their values evolve: with the increase in the O_2 percentage, they increase, except in the case of 15% O_2 for the tumble number.

Although some operating points are beyond the general tendency, the evolution of the integral length scale and the tumble number is smooth when the IMEP, equivalence ratio and O_2 percentage are varied. Thus, reasonable values of l_t and N_{tumble} can be obtained by interpolation of the data in look-up tables, in order to calculate transient engine operations.

3.2.2 Combustion Characteristics

The evolution of the calculated in-cylinder pressure at the stoichiometric equivalence ratio and IMEP = 1 000 kPa for

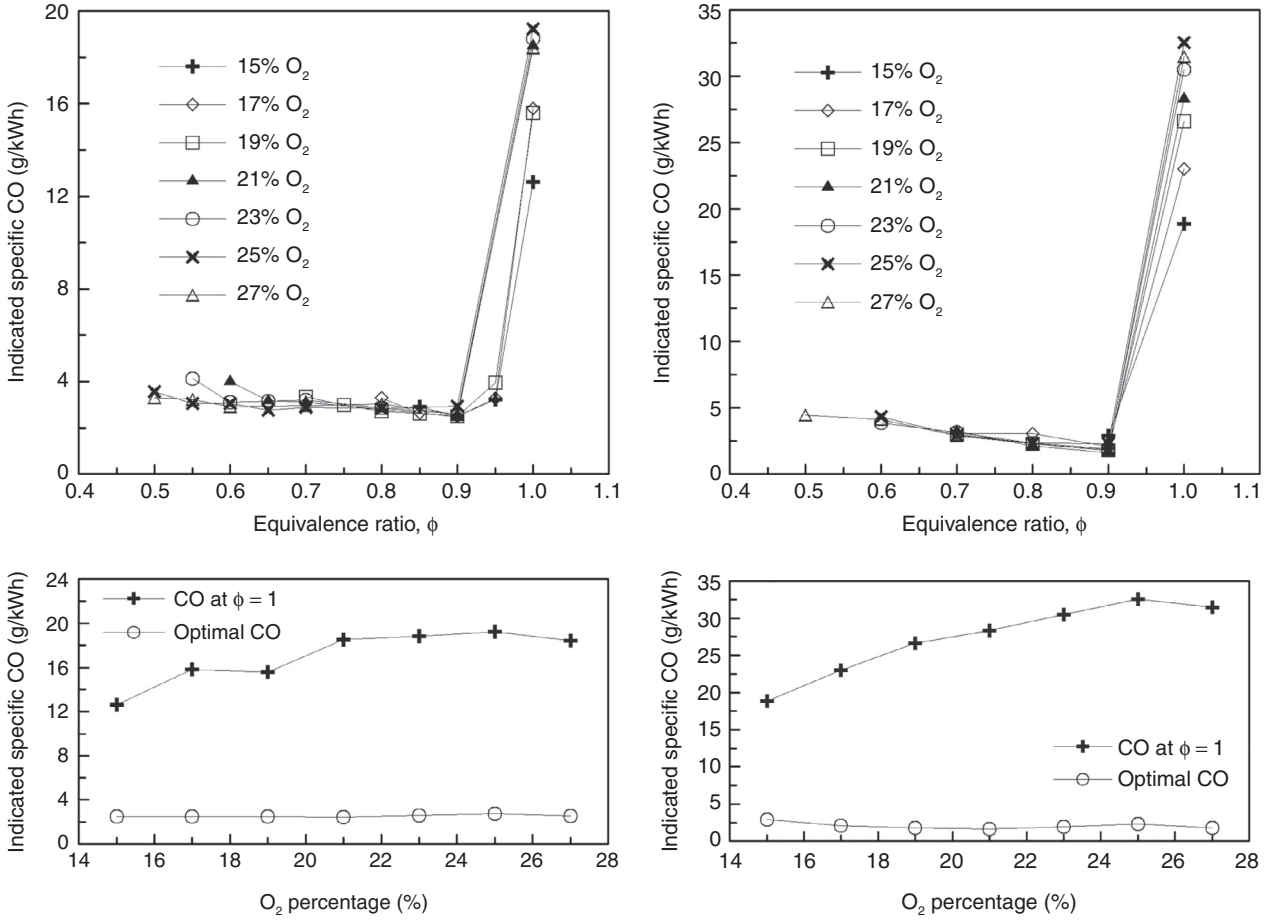

Figure 8

Evolution of indicated specific CO emissions *versus* the equivalence ratio for different IMEP; a) 400 kPa, b) 1 000 kPa).

different cases of the O_2 percentage is presented in Figure 12. The in-cylinder pressure is started at the spark ignition degree with the operation conditions listed in Table 4. The increase in the O_2 percentage results in a decrease in intake pressure while maintaining the same IMEP. However, for 27% O_2, in order to maintain IMEP at 10 bar, the intake pressure was kept at the same value as for 25% O_2 while increasing the spark timing to prevent knock. For relatively high O_2 percentages, engine operation was limited by knock phenomena, which can be seen in the in-cylinder pressure trace in Figure 12. To avoid engine knock, the higher spark timing was set for higher oxygen enrichment.

Figure 13 presents the laminar burning velocity evolution *versus* CAD with different O_2 percentages. The laminar burning velocity increases as a function of the O_2 percentage. Compared with 15% O_2, the laminar burning velocity of 27% O_2 is more than 8 times higher. The reasonable results of laminar burning velocity under engine operation conditions were obtained thanks to the reliability of the experimental correlation proposed by Galmiche *et al.* [24].

The evolution of the flame surface and flame wrinkling *versus* CAD for different O_2 percentages at the stoichiometric equivalence ratio and IMEP = 1 000 kPa are plotted in Figure 14. A previous experimental study (Mounaïm-Rousselle *et al.* [9]) showed that dilution enhances flame-turbulence interactions and that the corrugation generated through dilution occurs on smaller scales than the integral length scales. This phenomenon is well reproduced in the present simulation, as shown in Figure 14a, for 15 and 17% O_2, which correspond to 26.87% and 17.65% of EGR, respectively, as presented in Table 2. The flame surface is much higher than in the case of lower dilution

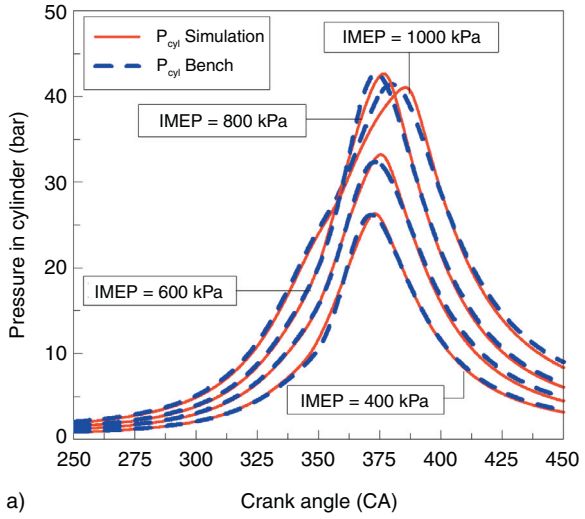

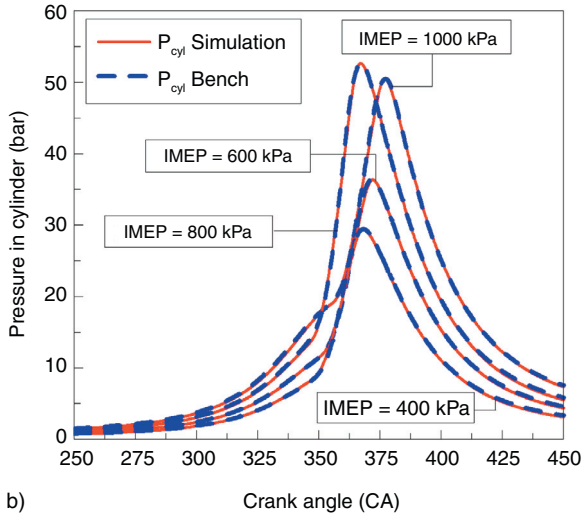

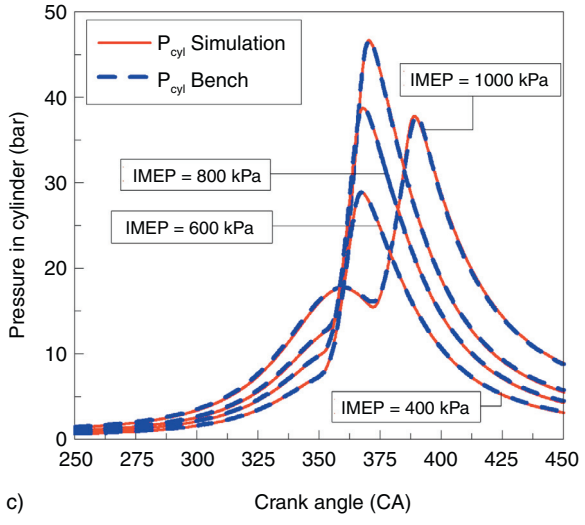

Figure 9

Comparison between experimental and simulated in-cylinder pressure evolution for different engine loads. φ = 1, a) 15% O_2, b) 21% O_2, c) 27% O_2.

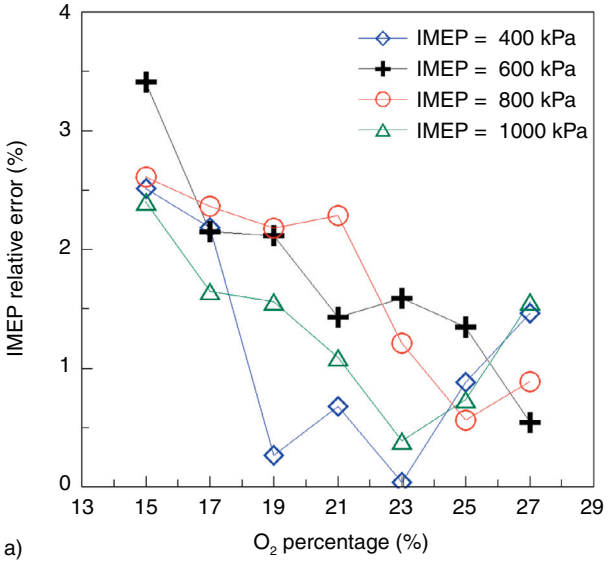

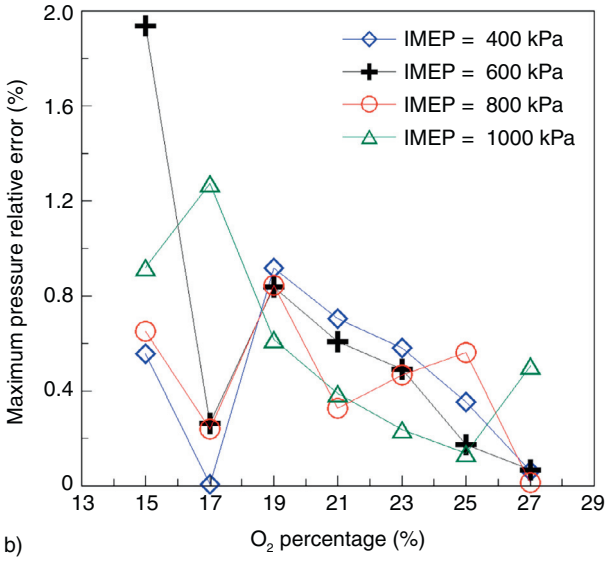

Figure 10

a) Relative error of IMEP and b) maximum in-cylinder pressure.

or oxygen enrichment. This tendency is mainly due to the high flame wrinkling in the case of high dilution, as presented in Figure 14b.

Finally, Figure 15 shows the evolution of the turbulent flame velocity *versus* CAD. The flame kernel growth is initially laminar-like as described in [27], and once the flame has grown to more than 5 mm, it can become turbulent [28].

Thus, based on the above findings, as the laminar burning velocity is much lower in the case of dilution, the laminar flame state lasts longer than with oxygen enrichment: about 7.5 CAD for 15% O_2, 5 CAD for 21% O_2 and 2.5 CAD for

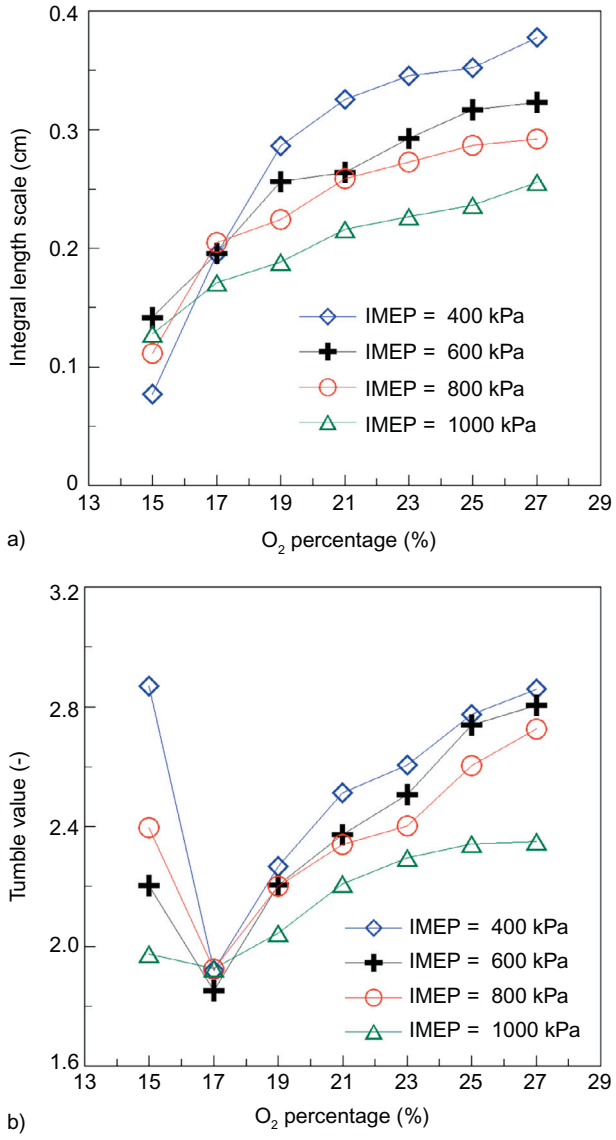

Figure 11

a) Integral length scale and b) tumble values obtained to optimize the in-cylinder pressure.

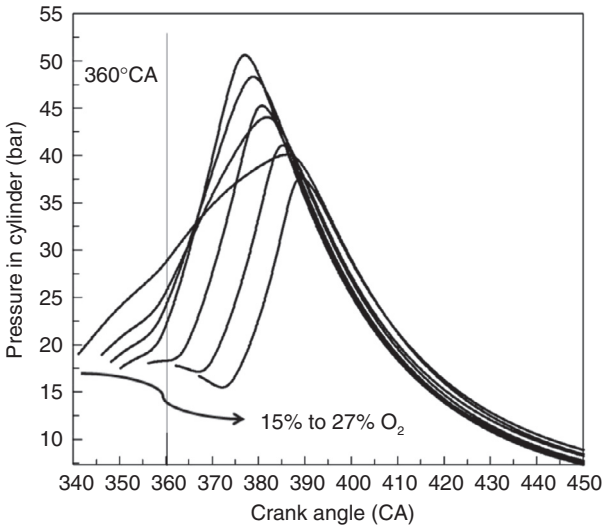

Figure 12

Evolution of the mean in-cylinder pressure at the stoichiometric equivalence ratio and IMEP = 1 000 kPa.

TABLE 4

Operating conditions for combustion analysis

O2 (%)	Intake pressure (bar)	Spark timing advanced (°CA)	Fuel mass flow rate (kg/h)
15	1.60	−19	0.98
17	1.39	−14	1.01
19	1.27	−12	1.05
21	1.19	−10	1.08
23	1.13	−4	1.12
25	1.12	2	1.19
27	1.12	7	1.28

27% O_2. Although substantial differences are found for laminar burning velocities (8 times higher with 27% O_2 compared with 15% O_2), the turbulent burning velocities show comparatively little difference (less than 2 times higher with 27% O_2 compared with 15% O_2). This is mainly due to the reverse evolution of flame wrinkling: the lower the O_2 percentage, the higher the flame wrinkling.

In order to characterize the combustion regime in the Peters-Borghi diagram [9], the evolution of the characteristic length and velocity scale ratio *versus* CAD for different O_2 percentages is plotted in Figure 16. As previously described, after the spark, the flame is initially 'laminar-like', and the duration of this phase is from about 2.5 to 7.5 CAD. Here, the curve starts at 10 CAD after spark timing (360 + ST + 10 CAD) for all the cases. A higher the value of l_t/δ_L is found for a higher value of the O_2 percentage; the reverse is true for u'/S_L. Two CAD cases of these ratios (10 CAD and 20 CAD after spark timing) are shown in Figure 17.

Finally, in Figure 18, the combustion is classified according the Peters-Borghi diagram, which gives a deeper insight into the interaction between turbulence and the flame front. According to the study of Linse *et al.* [29], engine

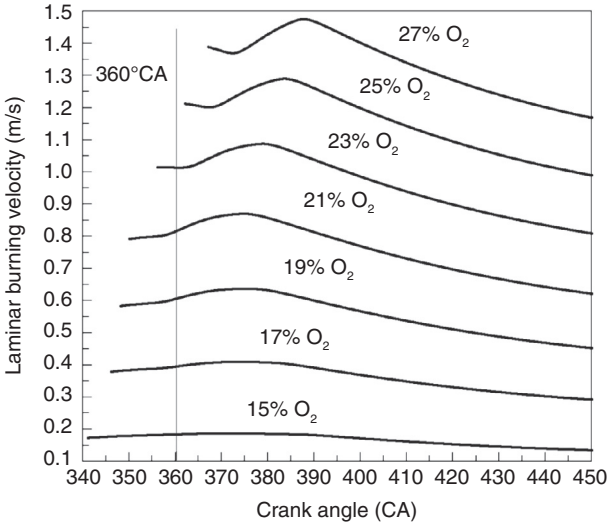

Figure 13

Laminar burning velocity *versus* CAD with different O_2 percentages at the stoichiometric equivalence ratio and IMEP = 1 000 kPa.

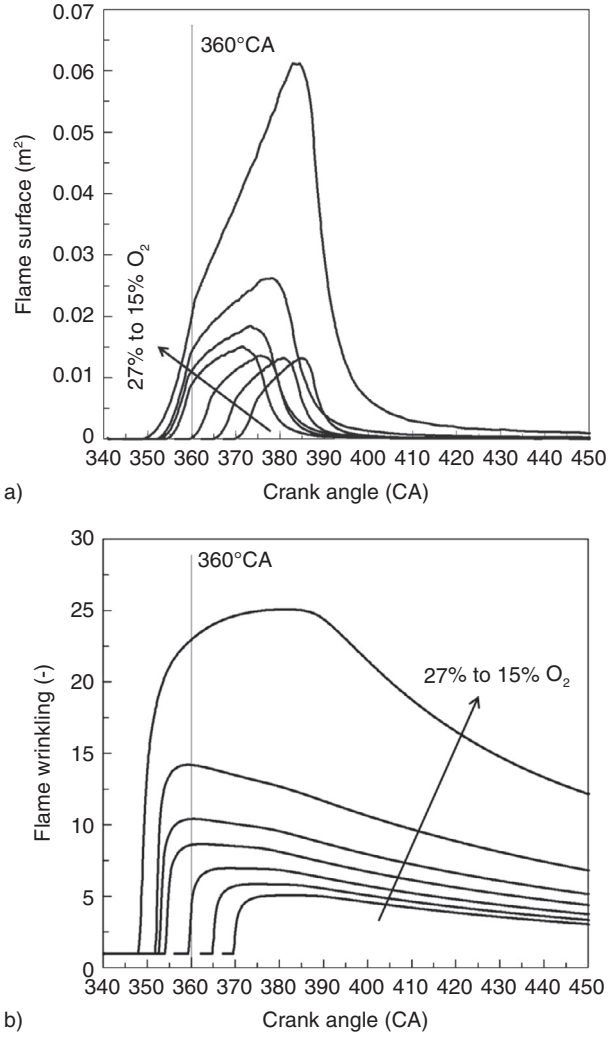

Figure 14

a) Flame surface and b) flame wrinkling *versus* the crank angle with different O_2 percentages at the unit equivalence ratio and IMEP = 1 000 kPa.

combustion is normally located in the thin reaction zone and the corrugated flamelet zone. Generally, the combustion of the earlier generation of SI engines takes place in the corrugated flamelet regime, while the combustion of the new generation of engines takes place in the thin reaction zone [30]. A higher turbulent level and charge motion are created when turbocharging and/or direct injection are used in new generation engines, which is the main reason for the different regime between new and earlier generation engines [29].

In Figure 18, from 15% O_2 to 27% O_2, the combustion trace passes from the broken reaction zone to the thin reaction zone, and finally to the corrugated flamelet zone. For the cases of 17% to 23% O_2, combustion takes place in the thin reaction zone, which may occur when the tested engine is supercharged and the high turbulence level is produced. For the cases of 25% and 27% O_2, the combustion traces are mainly in the corrugated flamelet zone, and for the case of 15% O_2, the combustion occurs in the broken reaction zone. Mainly, flamelet theory is used for engine combustion simulation, as validated by Poinsot *et al.* [31] based on direct simulation. Their results show that the resistance of the flame front to vortices is underestimated by classical diagrams which neglect viscous, transient and curvature effects. The limit line of the flamelet regime determined by Poinsot *et al.* [31] is drawn as the *v*-formed green line in Figure 18. Therefore, for the case of 15% O_2, the spherical propagation of the flame might not be well adapted, which certainly contributes to the imperfect agreement between simulated and experimental in-cylinder pressure (Fig. 9a).

The effect of N_2 dilution on the combustion trace corresponds well with the previous experimental study of Mounaïm-Rousselle *et al.* [9]. Dilution moves the combustion trace toward the upper left side in the Peters-Borghi diagram, and the effect of O_2 enrichment shows a reverse tendency compared with N_2 dilution. For all the operating cases, the combustion trace has a 'turning point'. Compared with the simulation results of Linse *et al.* [29], the 'turning angle' is smaller, which is caused by the simplification of the l_t definition in the AMESim model. l_t is supposed to be a constant value and equal to its value at spark timing

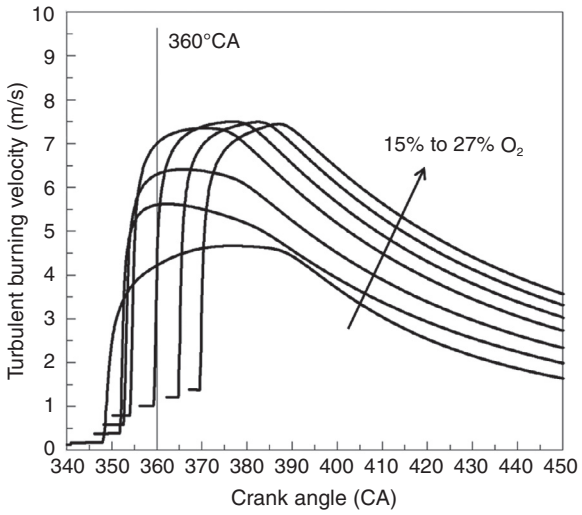

Figure 15

Evolution of turbulent flame velocity with different O_2 percentages at the stoichiometric equivalence ratio and IMEP = 1 000 kPa.

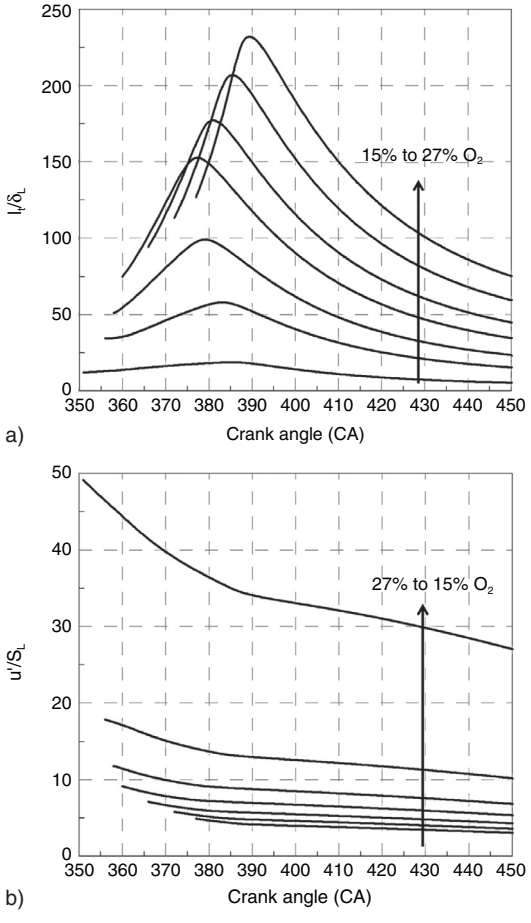

Figure 16

Ratio of the characteristic length a) and velocity scales b) *versus* CAD for different O_2 percentages.

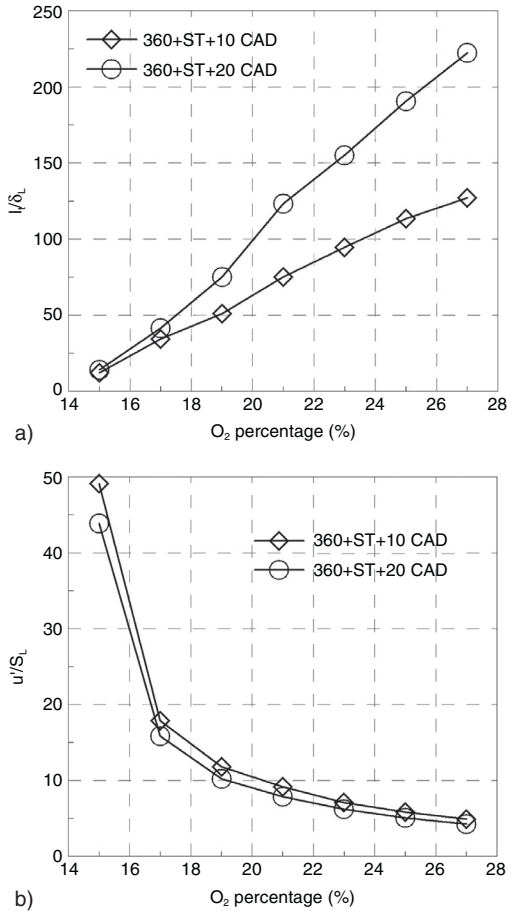

Figure 17

Ratio of the characteristic length a) and velocity scales b) *versus* the O_2 percentage for two CAD cases.

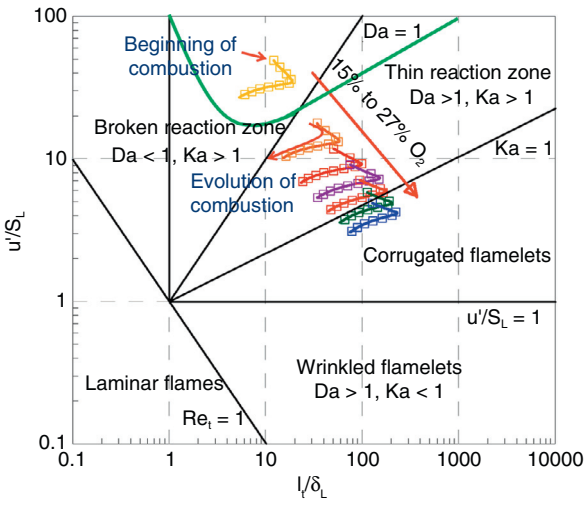

Figure 18

Comparison of the combustion traces in the Peters-Borghi diagram for different O_2 percentages.

during the whole combustion stroke in the combustion model [14], while l_t normally depends on the distance between the piston and cylinder head. Nevertheless, the general tendency is in good agreement with the previous studies of Linse *et al.* [29] and Mounaïm-Rousselle *et al.* [9].

CONCLUSION

In this study, the effect of controlling the oxygen concentration in the air on the performance and emissions in a downsized engine is presented and discussed, using both experimental and simulation methods.

The experimental results indicate that, by increasing the O_2 percentage in the air and decreasing the equivalence ratios, lower fuel consumption can be achieved for IMEP of 400 and 600 kPa. However, for 800 and 1 000 kPa, the lowest fuel consumption is obtained for 19% O_2 at 0.7 of the equivalence ratio and 15% O_2 at 0.9, respectively. It can be concluded that for low loads, oxygen enrichment has a real potential to improve fuel efficiency, whereas for relatively high IMEP, N_2 dilution still remains the best way. For all equivalence ratios, the HC emission decreases with the increase in the O_2 percentage and the lowest value can always be found at 27% O_2 but in this case, NO_x emissions increase.

The numerical simulation was conducted with the AMESim software by taking into account the effect of O_2 control. In-cylinder pressure was well reproduced, although discrepancies can be found for high levels of dilution. The increase in the O_2 percentage results in a decrease in intake pressure while maintaining the same IMEP. The laminar burning velocity increases as a function of the O_2 percentage. Compared with 15% O_2, the laminar burning velocity of 27% O_2 is more than 8 times higher. The flame surface of high dilution cases is much greater than that with lower dilution or oxygen-enriched cases. Therefore, turbulent flame velocities show few differences compared with laminar ones. The combustion trace passes from the broken reaction zone to the thin reaction zone, and finally to the corrugated flamelet zone by varying the O_2 percentage from 15% to 27%. Only for the case of 15% O_2 does the combustion take place in the broken reaction zone, in which the spherical propagation of the flame may not be well adapted.

ACKNOWLEDGMENTS

The authors acknowledge Stephane Richard for discussions to improve the AMESim software and the new procedure for residual gases. This study was financially supported by *PSA Peugeot Citroën* and Region Centre. This work was also financed by the MACDOC project of the French National Research Agency, TDM program, ANR-12-VPTT-0008. The authors are also grateful for the support from the Foundation of Zhejiang Educational Committee (No. Y201430810) and Natural Science Foundation of Zhejiang Province (No. LQ15E060001), China.

REFERENCES

1 Poola R.B., Ng H.K., Sekar R.R., Baudino J.H., Colucci C.P. (1995) *Utilizing Intake-Air Oxygen-Enrichment Technology to Reduce Cold-Phase Emissions*, Vol. **104**, New York, NY, Society of Automotive Engineers. 15.

2 Kajitani S., Clasen E., Campbell S., Rhee K. (1993) Partial-load and Start-up Operations of Spark-ignition Engine with Oxygen Enriched Air, *SAE Technical Paper* 932802.

3 Poola R.B., Sekar R., Ng H.K., Baudino J.H., Colucci C.P. (1996) *The effects of oxygen-enriched intake air on FFV exhaust emissions using M85*, Argonne National Lab., IL, United States.

4 Ng H.K., Sekar R.R., Kraft S.W., Stamper K. (1993) *The potential benefits of intake air oxygen enrichment in spark ignition engine powered vehicle*, Society of Automotive Engineers.

5 Caton J.A. (2005) Use of a cycle simulation incorporating the second law of thermodynamics: results for spark-ignition engines using oxygen enriched combustion air, *SAE Technical Paper* 2005-01-1130.

6 Poola R.B., Stork K.C., Sekar R., Callaghan K., Nemser S. (1998) Variable Air Composition with Polymer Membrane–A New Low Emissions Tool, *SAE Paper* 980178.

7 Kajitani S., Sava N., McComiskey T., Rhee K. (1992) *A spark ignition engine operated by oxygen enriched air*, Society of Automotive Engineers.

8 Quader A. (1978) Exhaust Emissions and Performance of a Spark Ignition Engine Using Oxygen Enriched Intake Air, *Combustion Science and Technology* **19**, 1-2, 81-86.

9 Mounaïm-Rousselle C., Landry L., Halter F., Foucher F. (2013) Experimental characteristics of turbulent premixed flame in a boosted Spark-Ignition engine, *Proceedings of the Combustion Institute* **34**, 2, 2941-2949.

10 Van Blarigan A., Seiser R., Chen J., Cattolica R., Dibble R. (2012) Working fluid composition effects on methane oxycombustion in an SI-engine: EGR *vs.* CO_2, *Proceedings of the Combustion Institute* **34**, 2, 2951-2958.

11 Favre E., Bounaceur R., Roizard D. (2009) A hybrid process combining oxygen enriched air combustion and membrane separation for post-combustion carbon dioxide capture, *Separation and Purification Technology* **68**, 1, 30-36.

12 Koros W.J., Chern R.T. (1987) *Separation of gaseous mixtures using polymer membranes*, Handbook of separation process technology, pp. 862-953.

13 Coombe H.S., Nieh S. (2007) Polymer membrane air separation performance for portable oxygen enriched combustion applications, *Energy Conversion and Management* **48**, 5, 1499-1505.

14 Richard S., Bougrine S., Font G., Lafossas F.-A., Le Berr F. (2009) On the reduction of 3D CFD combustion model to build a physical 0D model for simulating heat release, knock and pollutants in SI engines, *Oil & Gas Science and Technology - Rev. IFP* **64**, 3, 223-242.

15 *IFP Energies nouvelles* (2010) AMESim IFP Engine library user manual, LMS IMAGINE S.A.

16 Bougrine S., Richard S., Veynante D. (2011) On the combination of complex chemistry with a 0-D coherent flame model to account for the fuel properties in spark ignition engines simulations: Application to methane-air-diluents mixtures, *Proceedings of the Combustion Institute* **33**, 2, 3123-3130.

17 Bozza F., Gimelli A. (2004) A Comprehensive 1D Model for the Simulation of a Small-Size Two-Stroke SI Engine, *SAE Technical Paper* 2004-01-0999.

18 Richard S., Colin O., Vermorel O., Benkenida A., Angelberger C., Veynante D. (2007) Towards large eddy simulation of combustion in spark ignition engines, *Proceedings of the Combustion Institute* **31**, 2, 3059-3066.

19 Colin O., Benkenida A., Angelberger C. (2003) 3d Modeling of Mixing, Ignition and Combustion Phenomena in Highly Stratified Gasoline Engines, *Oil & Gas Science and Technology - Rev. IFP* **58**, 1, 47-62.

20 Charlette F., Meneveau C., Veynante D. (2002) A power-law flame wrinkling model for LES of premixed turbulent combustion Part I: non-dynamic formulation and initial tests, *Combustion and Flame* **131**, 1-2, 159-180.

21 Blint R.J. (1986) The Relationship of the Laminar Flame Width to Flame Speed, *Combustion Science and Technology* **49**, 1-2, 79-92.

22 Poulos S.G., Heywood J.B. (1983) The effect of chamber geometry on spark-ignition engine combustion, *SAE Technical Paper* 830334.

23 Zhou J.X., Cordier M., Mounaïm-Rousselle C., Foucher F. (2011) Experimental estimate of the laminar burning velocity of iso-octane in oxygen-enriched and CO_2-diluted air, *Combustion and Flame* **158**, 12, 2375-2383.

24 Galmiche B., Halter F., Foucher F. (2012) Effects of high pressure, high temperature and dilution on laminar burning velocities and Markstein lengths of iso-octane/air mixtures, *Combustion and Flame* **159**, 11, 3286-3299.

25 Friedman R., Johnston W.C. (1950) The Wall-Quenching of Laminar Propane Flames as a Function of Pressure, Temperature, and Air Fuel Ratio, *Journal of Applied Physics* **21**, 8, 791-795.

26 Mazas A.N., Fiorina B., Lacoste D.A., Schuller T. (2011) Effects of water vapor addition on the laminar burning velocity of oxygen-enriched methane flames, *Combustion and Flame* **158**, 12, 2428-2440.

27 Heywood J. (1994) *Combustion and its modeling in spark-ignition engines*, in *International symposium COMODIA*.

28 Boulouchos K., Steiner T., Dimopoulos P. (1994) *Investigation of flame speed models for the flame growth period during premixed engine combustion*, Society of Automotive Engineers.

29 Linse D., Hasse C., Durst B. (2009) An experimental and numerical investigation of turbulent flame propagation and flame structure in a turbo-charged direct injection gasoline engine, *Combustion Theory and Modelling* **13**, 1, 167-188.

30 Wirth M. (1993) *Die turbulente flammenausbreitung im ottomotor und ihre charakteristischen längenskalen*, in *RWTH Aachen*.

31 Poinsot T., Veynante D., Candel S. (1991) Quenching processes and premixed turbulent combustion diagrams, *Journal of Fluid Mechanics* **228**, 561-606, 230.

Manuscript submitted in March 2015
Manuscript accepted in September 2015
Published online in April 2016

Cite this article as: J.X. Zhou, B. Moreau, C. Mounaïm-Rousselle and F. Foucher (2016). Combustion, Performance and Emission Analysis of an Oxygen-Controlling Downsized SI Engine, *Oil Gas Sci. Technol* **71**, 49.